URN (Paper): urn:nbn:de:gbv:ilm1-2014iwk-081:7

58th ILMENAU SCIENTIFIC COLLOQUIUM
Technische Universität Ilmenau, 08 – 12 September 2014
URN: urn:nbn:de:gbv:ilm1-2014iwk:3

TRANSVERSAL VIBRATIONS OF BEAMS IN CONTEXT OF VIBRISSAE CONSISTING OF FOUNDATIONS, DISCRETE SUPPORTS AND VARIOUS SECTIONS

Daniel Baldeweg / Christoph Will / Carsten Behn

Department of Technical Mechanics
Ilmenau University of Technology
Max-Planck-Ring 12 (Building F)
98693, Ilmenau, Germany
{daniel.baldeweg, christoph.will, carsten.behn}@tu-ilmenau.de

ABSTRACT

In this paper, we deal with the transversal vibration analysis of beams. Based on mechanical models which are inspired by the vibrissae of rats and mice, a contribution to the distance detection using these mechanical sensors is made. Already existing models from literature are improved and designed more realistic: the elasticity of the follicle-sine-complex (FSC, support of the vibrissa), of the skin, and the conical shape of the vibrissa are taken into account, and their impact on the dynamic analysis is determined. The FSC is modeled by a viscoelastic-foundation, the skin by a discrete spring-damper-combination, the conical shape by three different diameters, and the object contact point by a (fixed) bearing. Furthermore, different types of supports (clamping, bearing and free end) are considered. Due to the complexity of the models, we firstly focus on conservative systems in this paper (three models are studied). As mentioned, these models differ from each other only by the type of support. For the obstacle distance detection, we set up two algorithms to unambiguously determine the object distance with the help of some eigenvalues (later measured in experiments) of the boundary-value system (i.e., partial differential equation with boundary conditions). This is firstly done in deriving the context of the transition points between ω_i and ω_{i+1}, and secondly in establishing the functions of the displacements $v_i(x,t)$ with the help of the relationship between the eigenvalues and the natural frequencies. Finally, the influence of the discrete spring on the behavior of the eigenvalues is presented, and the algorithms are tested to be valid for the developed models.

Index Terms— tactile sensor, bio-inspired sensor, animal vibrissa, distance determination, object localization, natural frequency

1. INTRODUCTION

There is a great interest in tactile sensors, since they have advantages in contrast to other sensor types. They are superior to optical sensors, for example in the dark, murky water or in smoky air, and also cheaper in manufacture and use. In the development, engineers often use biological systems as an inspiration. A tactile system, which attracted attention in recent years, is the *vibrissa* of rats and mice, see Fig. 1 (left). They use their vibrissae, e.g., to distinguish between different surfaces or to recognize textures and edges, respectively. There are already various mechanical models for a vibrissa to explain the technical acquisition of information.
The scope of the present paper is to contribute to the mechanical modeling of a technical vibrissa as tactile sensors for the distance detection.

1.1. Vibrissae

Vibrissae are a particular type of hair which occur in most mammals (an exception is the human being, who possesses no vibrissae [16], [1]). Commonly, these are also called whiskers and the term is *Pilus tactilis* [21], [27]. They can occur at different areas of the body, for example, on the forearms, near the lips and eyes [1]. Most studies have concentrated on vibrissae near lips of rats and mice, which are called *mystacial vibrissae*. The mystacial

vibrissae are arranged in a specific manner in the snout region of rats and mice: they form arcs and rows [8]. The rows are denoted from dorsal to ventral with letters and the arcs from caudal to rostral with numbers [20], see Fig. 1 (right).

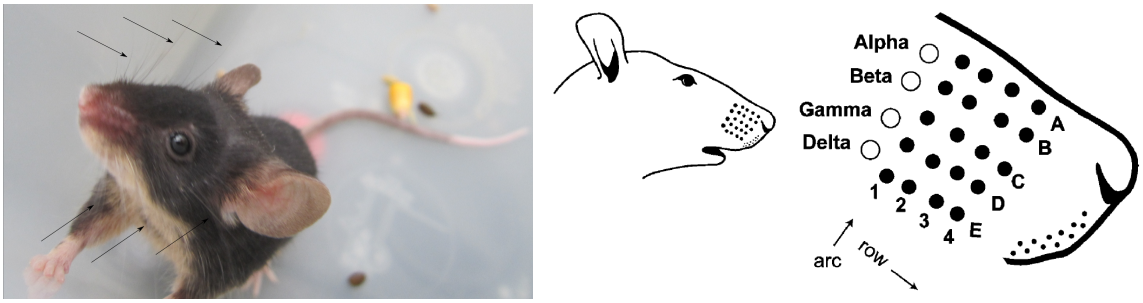

Figure 1. Vibrissae (see arrows in the picture) of the mouse "Lilly" (left); mystacial pad [33] (right).

Remark 1.1. *The following descriptions largely refer to the mystacial vibrissae. In addition, the focus is on a single vibrissa in the later calculations, not on the whole field of vibrissae.* ◇

Vibrissae differ from an ordinary hair by their larger diameter and greater length [21]. Further, vibrissae are slightly curved, hollow and have a conical shape [33]. Furthermore, the vibrissa is surrounded by a blood sinus beneath the skin [21], [20], see Fig. 2 (left). There are different assumptions about the function of the sinus [20]: one is, that due to the change of the blood pressure in sinus, the animal can adjust the stiffness of the support of the vibrissae [8]. Thus, the mouse or rat could actively adjust the vibrissae to the environmental conditions [29]. The hair follicle and the blood sinus build together the *follicle-sine-complex* (FSC).
There are different types of *mechanoreceptors* within the FSC, which can measure stress, strain and vibration stimuli, see Fig. 2 (left). For example, Merkel cells can detect compression stimuli [20]. Thus mechanical stimuli can be realized and converted into information, but how is still unknown (and this does not matter for the investigation of this work).
The mystacial vibrissae can be moved through the *extrinsic* and/or *intrinsic muscles*. The extrinsic muscles belong to the group of facial muscles and have their origin outside of the mystacial region. The intrinsic muscles form a loop around the lower third of the hair follicle and connect two consecutive vibrissae. The hair follicles are interconnected by a *fibrous tissue* and placed in the fat tissue, so that they can move freely [10], see Fig. 2 (right).

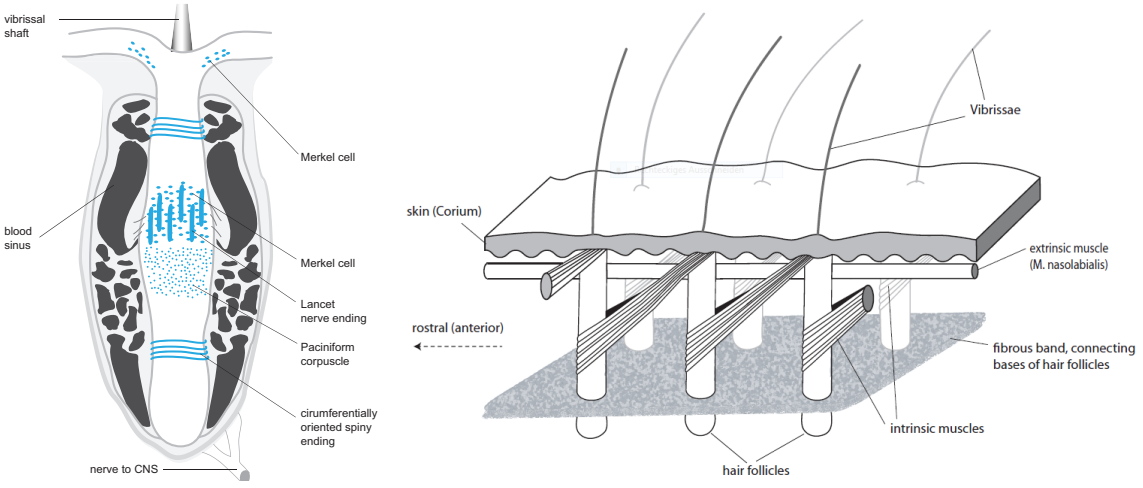

Figure 2. FSC with blood sinus and mechanoreceptors [2] (left); Representation of the musculature of the vibrissa [3] (right).

Rats and mice can move their vibrissae in special patterns [1]. Therefore, one can distinguish between a passive and an active mode for the mystacial vibrissae:

1. *passive mode*
   In the passive mode, the vibrissa is deflected from its rest position by an external force and, after the disap-

pearance of the external force, the vibrissa returns passively to its original position through the fibrous tissue [29], [8].

2. *active mode*
   In the active mode, the vibrissa is moved by the intrinsic and/or extrinsic muscles. The extrinsic muscles generate a movement in the caudal direction (retraction), while the intrinsic muscles produce a movement in the rostral direction (protraction) [6]. These two possibilities can explain the two patterns of the vibrissae movement, also called whisking:

   - *exploratory whisking:*
     The vibrissae are moved with a large amplitude and small frequency between 5-15 Hz. The protraction results from the intrinsic muscles and the retraction from the extrinsic ones. Thus, the retraction is an active process [6]. This pattern is used for the exploration of the environment, e.g., for scanning contours and edges [29], [8].
   - *foveal whisking:*
     The vibrissae are moved with a small amplitude and large frequency between 15-25 Hz. The protraction results from the intrinsic muscles and the retraction from the fibrous tissue. Thus, the retraction is a passive process [6]. This pattern is used for a closer examination of objects, e.g., for texture recognition [29], [8].

How the movements in the passive or active mode are converted into information about the environment is not yet clearly understood. An essential fact is that the vibrissae have no receptors along their hair shaft, but that the receptors, which can obtain information and then transmit this information through the neural pathways, are only located in the blood sinus.
One possibility is, that the natural frequencies of the vibrissae could play a role in the texture recognition. Thus, it has been shown that textures can be distinguished by two vibrissae with a different natural frequency spectrum [24].

1.2. Modeling

There are different approaches for the mechanical modeling, which are used to analyze the vibrissa mechanically and to investigate the properties:

1. *rigid-body model*
   The vibrissa consists of a finite number of bodies, coupled physically and/or geometrically with each other, [4], [29], [28]. But, every body is rigid and therefore not deformable. The simplest model is that the vibrissa consists of one body. However, this model has the disadvantage that the elasticity of the vibrissa is completely neglected. By contact with an object, the vibrissa is bent. So, with this model, only a part of the properties or functions of the vibrissa can be explained.

2. *continuum model*
   In this model, the vibrissa is modeled as a beam. Within the bending beam models, different beam theories can be distinguished. The two best known are the Euler-Bernoulli beam theory and the Timoshenko one. For the vibrissa (major length to minor diameter) the Euler-Bernoulli beam theory is almost exclusively used. Basically two types of examination, the static and dynamic analysis, can be differed:

   - *static analysis*
     On the basis of forces and moments at the base support, the shape or the point of contact between the vibrissa and the object is determined.
   - *dynamic analysis*
     On the basis of the natural frequency spectrum, information about the environment is obtained, e.g., where the contact point is and which roughness the surface has.

For the modeling of the vibrissa in this study, the continuum model is used. Therefore, in Chapter 2, the recent continuum models of a vibrissa from the literature are presented. The focus is on the vibration analysis (dynamic analysis).

1.3. Goal

In the present paper, mechanical models of animal vibrissae — already existing in the literature — are improved and made more realistic. Hence, the FSC, the skin and the conical shape are considered and their impact on the dynamic analysis can be determined. Furthermore, different types of support can be examined. Afterwards, information about the environment is derived by using natural frequencies. Here, we focus on the determination of the contact point between the vibrissa and the object. This contact point is calculated by using an algorithm and parts of the natural frequency spectrum.
The focus is not on using the mechanical model to explain the characteristics and functions of the biological system of the vibrissae. Rather, the focus is on the vibrissa as an inspiration (bionics): Starting with the vibrissa a mechanical model is created and based on this, relationship and properties are investigated. Ultimately, this study will contribute to the development of tactile sensors.

2. STATE OF ART

As mentioned in Chapter 1, it is not yet clearly understood, how the information gathering occurs, but concerning the mechanical parameters that are measured by the receptors, there are several hypotheses:
One hypothesis is that the forces and moments measured with the receptors in the blood sinus can be used to determine the contact point along the vibrissa and the torque curve, which is caused by the movement of the vibrissa over the surface, can be used to differ between different surface structures.
In addition to the forces and moments, the vibration of the vibrissae, which occur when touching an object, could be used as well (vibration analysis). The vibrissa has a natural frequency spectrum and by contact this spectrum is shifted. This information could be used to determine the contact point along the vibrissa. Furthermore, there are vibrissae with different lengths and diameters and so with a different natural frequency spectrum. If different vibrissae are moved over the surface, the surface structure could be determined due to the different effects on the vibration behavior.
In the following, a brief insight into the vibration analysis of a vibrissa is described. The reader's attention is invited to, e.g., [7], [31], [14], or [30], to get some insights on the static analysis. Finally, the models for the vibration analysis are summarized.

2.1. Dynamic analysis

2.1.1. Model 1

In [24], the vibrissae are seen as thin elastic beams with a conical shape. The formula for the natural frequencies for free vibrations is:

$$\omega_n = \frac{\kappa_n^2}{2\pi} \frac{r_{base}}{L^2} \sqrt{\frac{E}{\rho}}, n \in \mathbb{N}, \tag{1}$$

where r_{base} is the radius at the base of the hair, L is the length of hair, ρ is the density of the hair, and κ_n is a constant. This constant depends on the boundary conditions and the shape of the hair. In κ_n the eigenvalue is included, which can be determined by the eigenvalue equation. Vibrissae, which are located on a living mouse, and vibrissae, which have been removed from a mouse and have been clamped, were set into vibration by a piezoelectric actuator and the first natural frequency has been determined. Subsequently, E and κ_1 were estimated from these data. After that the first natural frequency of each vibrissa in the mystacial pad of a mouse was experimentally determined and compared with the calculations based on the model. It is shown that the experimentally determined and the calculated values differ, see Fig. 3. If the vibrissa is excited with a frequency near the natural frequency, the amplitude of the oscillation movement is increased. If the vibrissa is moved over a surface texture, vibrations of the vibrissa are generated. The frequency of the vibration depends on the speed of movement and the surface structure. Thus, the amplitude of the oscillation movement is increased when the frequency of oscillation is near the natural frequency of the vibrissa. Due to the large span of the natural frequencies of the field of vibrissae, the mouse could determine with a single vibrissa whether a surface is rather smooth or rough. If the mouse uses several vibrissae at the same time, the mouse could determine more precisely the surface texture by the difference of the amplitude between two rows of vibrissae [24].

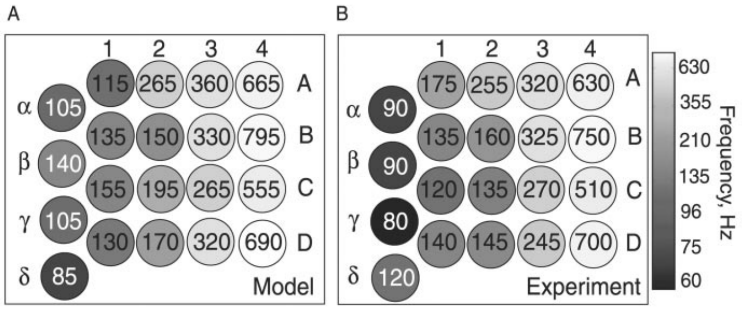

Figure 3. Comparison of the experimentally and numerically calculated first frequency [24].

2.1.2. Model 2

The model in [32] is called "dynamic antenna". It is a flexible beam with a constant cross section and a mass at the tip. With help of the first and second natural frequency of the beam, the contact point with an object can be determined. As the name already indicates, this is not a model for a vibrissa, but one for the long antenna of insects. Nevertheless, the model can also be applied to vibrissae by setting the mass of the tip equal to zero. One end of the beam is considered to be clamped while the other can vibrate freely. A contact with an object along the length of the beam is regarded as being held temporarily.

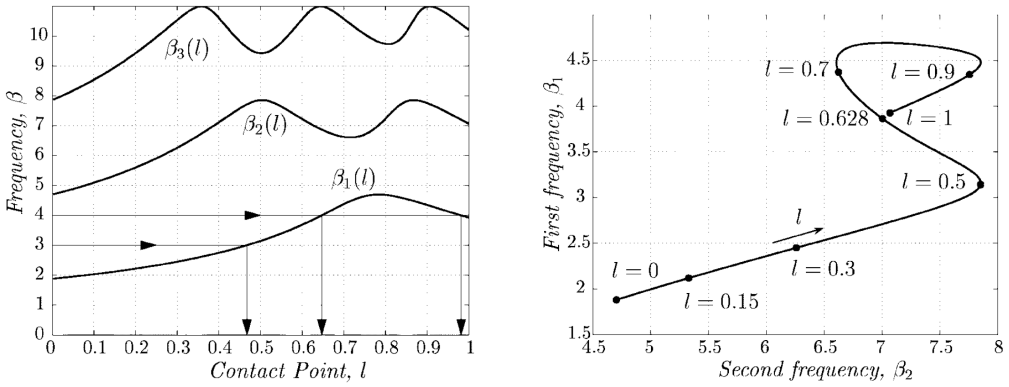

Figure 4. The first three natural frequencies (left); the first frequency vs. the second frequency (right) [32].

It turns out that the natural frequency curve does not have a strict monotonic behavior, see Fig. 4 (left). Thus, for a certain value, the contact point cannot be determined uniquely by only one natural frequency curve. But, if a spectrum of the natural frequencies is known, the contact point can be determined unambiguously. The authors also show, that an unambiguous determination of the contact point is possible by using the first two natural frequencies, see Fig. 4 (right). Thus, the system "dynamic antenna" can determine the distance of an object with the help of the first two natural frequencies.

Remark 2.1. *In Figure 4 (right), it can be seen, that the curve almost has an intersection. In [32], the authors expanded the curve with the mass at the tip, in this paper an attempt is made to expand the curve by a change of parameters.*

2.1.3. Model 3

The model in [19] is similar to the model in [32]. The authors also used a beam with a constant cross-section, but the beam posses no mass at the tip, since this model has been developed directly for the vibrissa. Based on their model they create an artificial vibrissa. They experimentally checked on the one hand the run of the natural frequency curves in contact with an object, and on the other hand they performed experiments on the ability of the surface discrimination. It is found that for the first three natural frequencies the calculated values match well with the experimental data. However, the higher natural frequencies show larger differences. An explanation for

this could be the damping, which has not been considered [19]. In a next step, it was checked whether surfaces discrimination with the artificial vibrissa is possible. It has been found, that the best results have been obtained with short vibrissae, which had a small diameter and were moved fast over the surface. This could explain why the mice and rats use small vibrissae on their snout, called microvibrissae, for texture recognition [19].

2.1.4. Model 4

In the model of [36], the vibrissae have a conical shape, as in [24]. A special feature of this model is the support of the vibrissae. Both the base and the tip of the vibrissae are supported by two springs, a translational and rotational one, see Fig. 5.

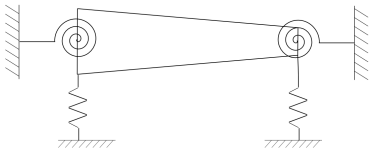

Figure 5. Model of the vibrissa from [36].

These support conditions are in a high contrast to those of previous models, which have held the base of the vibrissa clamped. However, they reflect the reality not yet precise enough. Therefore, in this work, the support conditions are modeled more realistic. With help of the spring constant $k_{t,b}$ for the translatory spring and $T_{t,b}$ for the rotary spring, several special cases can be generated. Whereas t is the spring at the tip and b is the spring at the base. So one get a free end for $k_{t,b}, T_{t,b} = 0$ and a clamping for $k_{t,b}, T_{t,b} \to +\infty$.
In the analysis of this model, one can see very well that not only the support conditions, but also the ratio of the radii has influence on the natural frequency. The natural frequency has been calculated for different spring constants of the base using real data from a vibrissa. This has the background that probably the mouse can actively change the support conditions of the base with the help of the FSC. There is an area that is around $3 \cdot 10^{-7}$ Nm/rad to $3 \cdot 10^{-5}$ Nm/rad, in which a change of k_b has only a small effect on the natural frequency, while the natural frequency is very sensitive to a change of T_b. If T_b is increased in this area, the natural frequency decreases sharply. This means that a rat or mouse might change the natural frequency of individual vibrissa by an increase or decrease of the rotational spring constants. This suggests that the resonance of vibrissae could play a role in the texture recognition [36].

2.1.5. Model 5

In this model of [17], as in the model of [36] and [24], the vibrissa has a conical shape, but with a clamping at the base and a free tip. In [17], the vibration behavior of vibrissae is inspected, which were removed from rats and fixed with glue to a vibration table, and of vibrissae of living rats. However, the glue has damping properties, and thus could distort the results. With help of the vibrissae attached on the vibration table they have analyzed to what extent the experimentally determined natural frequencies coincide with the numerically calculated natural frequencies and thus, whether the model of vibrissa as a truncated cone is applicable. Furthermore, they have examined the vibration behavior of vibrissae on living rats.
For the first three natural frequencies the measured values are 40, 94 and 188 Hz and the numerically calculated values are 47, 115 and 213 Hz. This shows that the experimentally determined values are less than the calculated values. One reason could be the attachment with the glue. Subsequently, the vibration behavior of vibrissae of living rats was examined. On the one hand the natural frequencies were smaller, and on the other hand a higher damping occurred. This can be attributed to the difference in the boundary conditions. In the experiment with the vibration table, the vibrissae have been attached to the table, while in the rat the vibrissae are held in the FSC. Furthermore, the rat seems to be able to actively vary the natural frequency and the damping of a individual vibrissa with the help of the FSC, because different degrees of damping and different natural frequencies of an individual vibrissa have been observed [17].

2.1.6. Models at the TU Ilmenau

In [4], different models for the vibrissa were studied. The influence of various system parameters to the natural frequencies were analytically analyzed. In the following, two models are shown:

In the first model – *Model 6* – both the skin and the support in the FSC are considered through a spring-damper pairing, see Fig. 6(left).

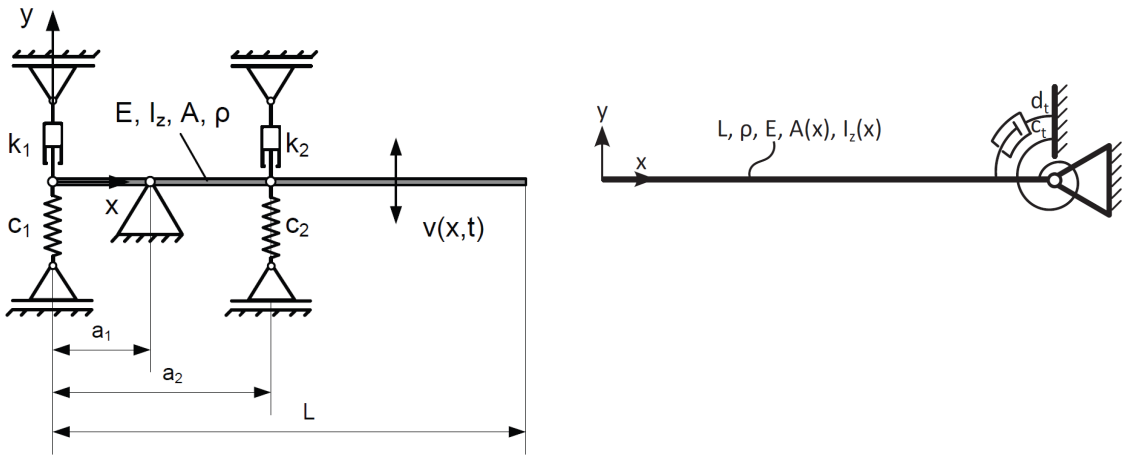

Figure 6. Two models of a vibrissa [4].

Here, an influence on the natural frequencies by the two spring constants c_1 and c_2 and the two distances a_1 and a_2 was found. Furthermore, the natural frequencies decrease because of the damping, but with an unlike behavior, see [5].
In another model – *Model 7* – the complete FSC is assembled with a fixed bearing, a rotational spring and a rotational damper, see Fig. 6(right).
It was shown that by an increase of $c_t \rightarrow +\infty$ or $d_t \rightarrow +\infty$ the oscillation behavior matches with that of a clamping. In addition, the natural frequencies only changed marginal, if c_t or d_t are above a certain value. Below this range, the biggest change occurs.

2.1.7. Robots with vibrissae

In [25], a robot rat which can discriminate textures by using his vibrissae is developed. For that the robot rat has a vibrissae field on both sides, which is based on the vibrissae field of a rat. The deflections of the individual vibrissa are collected in order to determine the product of the amplitude and frequency of the signal with the help of an algorithm. It is believed that by a rat this product is directed to the brain.
In a first experiment, the position of the rat is fixed and only the head can whisk the vibrissae field over the eight different surfaces (eight different gainings of sandpaper). The more vibrissae were used, the better the texture recognition was. Looking at the results of the individual arcs, where as in [24] the vibrissae within the same arc have about the same natural frequencies and there are differences in the natural frequencies between the arcs, it has been shown that certain arcs have achieved better results by certain surfaces than other arcs. This suggests that the natural frequency of the individual vibrissa could play a role in surface recognition [25].
In a second experiment, the position of the rat is no longer fixed. The robot rat has to go through a corridor and has to distinguish between four textures, without moving the head. Depending on the texture combination within the corridor the robot rat has to turn right or left autonomously. Just by the result of the algorithm, the robot rat turned right or left autonomously depending on the texture combination.

2.2. Conclusion

Finally, the mechanical models for the vibrissa used in the vibration analysis are compared in terms of their similarity to the real vibrissa.
Model 2 and 3 represent the most abstract model. The vibrissa is considered as a cylindrical beam and the FSC as a clamping. Model 1 and 5 represent the FSC as a clamping, but assumes a conical shape of the vibrissa. Model 4 does not use a clamping, but springs. With this, the conditions of support can be changed by using the spring constants. Model 7 is similar to Model 4. Instead of a clamping a bearing, a rotational spring and a rotational damper is used. In Model 6 the FSC is considered in more detail. There is a spring-damper pairing for the blood sinus and a pairing used for the skin. Thus, Model 4, 6 and 7 are a first step to simulate the actual support in the FSC.
Overall, several forms for the vibrissa have been considered and there have been first approaches to the modeling

of the support conditions in the FSC, but the bearing in the FSC requires a more detailed examination, as this could play a crucial role in stimulus detection. An assumption is that the support conditions can be actively changed to suit the vibrissa to the running task.

3. CONCRETION

In this paper, the Euler-Bernoulli beam theory is used. Exclusively a consideration of the dynamic analysis (vibration analysis) is done and linear models are used. The already existing models in the literature have shown, that although there are approaches to simulate the real support of the vibrissae, they are still very far from reality. Furthermore, the skin has not been taken into account. Therefore, known models in the literature are enhanced and improved. Thus, complex models are created, which better reflect the actual properties and support conditions of the vibrissae. These models, for example, have the ability to change the support conditions with help of the spring constant, because probably the mouse or rat also has this facility.
With help of the models the influence of FSC, skin, conical shape and modification of support on the dynamic analysis can be determined. Furthermore, it is investigated, to what extent models that depict the biological model in more detail, are better suited for distance detection.
The previous investigations of tactile sensors have used a cantilever beam with a point mass at the tip as a model. The investigations in this paper extend the results of the literature in order to develop further options for the design of tactile sensors.

4. MODELING

In this chapter the modeling of the vibrissae is discussed. It is shown which parts of the vibrissa can be modeled by means of mechanical components. Subsequently, for the technical vibrissa a set of parameters is presented.

4.1. Modeling

Figure 7 shows how the vibrissa is converted into a mechanical model:

- Properties of the FSC $\rightarrow$ viscoelastic-foundation (adjustable)
- Influence of skin $\rightarrow$ discrete spring-damper combination
- Object contact point $\rightarrow$ short-term bearing
- Conical shape $\rightarrow$ three cross sections
  (D_1 - diameter in the FSC, D_2 - diameter between FSC and skin, and D_3 - diameter outside the skin)

Since this model is very complex, it is broken down for further calculations into smaller sub-models. A first classification is based on conservative systems, which are presented in Chapter 5, and non-conservative systems, which are not analysed in this paper. Within this classification a further breakdown by type of support at the base is made:

- Model A: at $x = 0$ a clamping,
- Model B: at $x = 0$ a bearing, and
- Model C: at $x = 0$ a free end as well.

4.2. Parameter set for the vibrissa

For the model, different values are needed to calculate the natural frequencies and eigenvalues for the dynamic analysis. Therefore, a parameter set is created. Since the goal is not the replica of biology, but the understanding of influences and relationships, a technical set is used. This data are unrealistic for the vibrissae of rats, but they represent the relationships better and can be considered as parameters for a tactile sensor.

Technical set
In the technical set a steel beam is used:

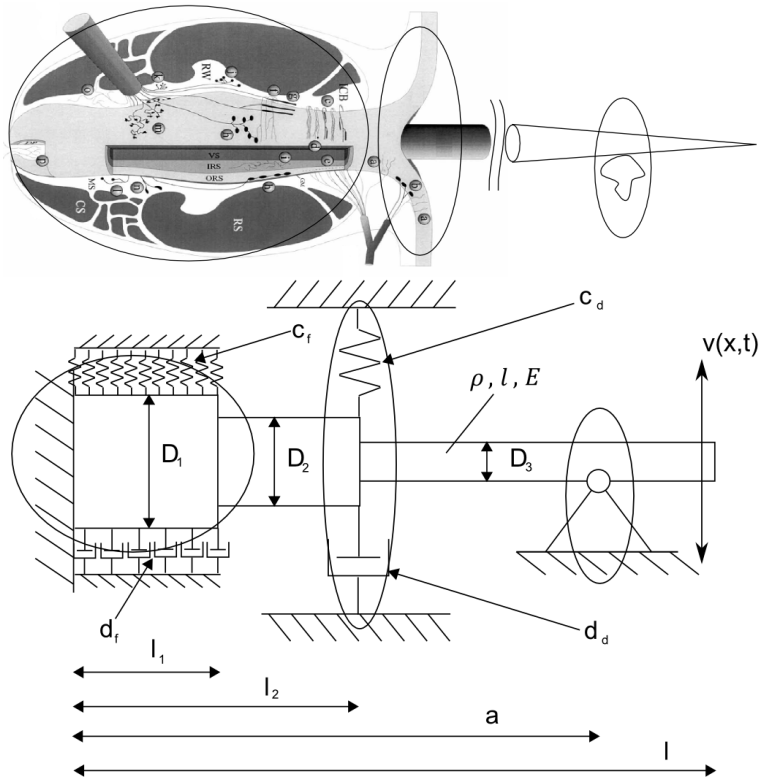

Figure 7. Modeling of a vibrissa: above - vibrissa with contact [12]; below - model of a vibrissa with contact.

Table 1. Technical set.

ρ	7850 $\frac{\text{kg}}{\text{m}^3}$
E	210 GPa
$D_1 = D$	10 mm
D_2	7.5 mm
D_3	5 mm
l_1	250 mm
l_2	500 mm
l	1000 mm

5. CONSERVATIVE SYSTEMS

In this chapter, three conservative models for the vibrissa are presented. For each model the first three eigenvalues are calculated and the possibility of a distance detections is checked. In addition, the influence of the discrete spring is examined.
For all calculations, Euler-Bernoulli beam theory is used and the following conditions and assumptions were made:

- straight beam (no pre-curvature),
- linear elastic material behavior (HOOKE's law),
- small strains, and thus small deformations,
- plane sections remain flat in the deformation and the cross sections are perpendicular to the axis of the beam (BERNOULLI-Hypothese) [18], [22], [35], [15], [11],
- free vibrations, i.e., the beam is excited once by an impulse,
- E, ρ, I_z and A constant over the length of the beam or constant in sections.

The equation of motion of a beam with a spring foundation is, see [13], [26]:

$$\rho\, A\, \ddot{v}(x,t) + E\, I_z\, v''''(x,t) + c_f\, v(x,t) = 0, \tag{2}$$

where $v(x,t)$ is the vertical displacement at point x and time t in the y-direction (see Fig. 7), E is the modulus of elasticity, I_z is the second moment of area, A is the cross section area, ρ is the density of the material and c_f is the spring rate of the foundation. The solution of (2) is found by using the method of separation of variables with the following approach:

$$v(x,t) = X(x) \cdot T(t),\ \forall (x,t),$$

resulting in the following equation:

$$\frac{\ddot{T}(t)}{T(t)} = -k^4\, \frac{X''''(x)}{X(x)} - \frac{c_f}{\rho\, A}. \tag{3}$$

Equation (3) shows that the left-hand and right-hand sides, for each time t and for each location x, must be the same and, therefore, constant. The constant is set to $-\mu^2$. Subsequently the partial differential equation can be split into two ordinary differential equation. The first differential equation is:

$$\begin{aligned} \frac{\ddot{T}(t)}{T(t)} &= -\mu^2, \qquad \mu \in \mathbb{C} \\ \ddot{T}(t) + \mu^2\, T(t) &= 0, \end{aligned}$$

with solution:

$$T(t) = \tilde{C}_1\, e^{i\mu t} + \tilde{C}_2\, e^{-i\mu t}, \qquad \tilde{C}_1,\ \tilde{C}_2 \in \mathbb{C}.$$

With $\mu = \mu_{re} + i\,\mu_{im}$, $\tilde{C}_1 = \tilde{C}_{1,re} + i\,\tilde{C}_{1,im}$ and $\tilde{C}_2 = \tilde{C}_{2,re} + i\,\tilde{C}_{2,im}$ we have:

$$\begin{aligned} T(t) = {} & e^{-\mu_{im} t}\, \tilde{C}_{1,re}\, \cos(\mu_{re} t) - e^{-\mu_{im} t}\, \tilde{C}_{1,im}\, \sin(\mu_{re} t) \\ & + e^{\mu_{im} t}\, \tilde{C}_{2,re}\, \cos(\mu_{re} t) + e^{\mu_{im} t}\, \tilde{C}_{2,im}\, \sin(\mu_{re} t) \\ & + i \Big(e^{-\mu_{im} t}\, \tilde{C}_{1,im}\, \cos(\mu_{re} t) + e^{-\mu_{im} t}\, \tilde{C}_{1,re}\, \sin(\mu_{re} t) \\ & \qquad + e^{\mu_{im} t}\, \tilde{C}_{2,im}\, \cos(\mu_{re} t) - e^{\mu_{im} t}\, \tilde{C}_{2,re}\, \sin(\mu_{re} t) \Big). \end{aligned}$$

As a free vibration is existent, the energy cannot increase, so the following results, see [34]:

$$T(t) = C\, e^{i|\mu| t}, \qquad C \in \mathbb{C},$$

and, for the real part of the function, we have, see [4], [34]:

$$T(t) = e^{-|\mu_{im}| t}\, \left(C_1\, \cos(|\mu_{re}|\, t) + C_2\, \sin(|\mu_{re}|\, t) \right), \qquad C_1,\ C_2 \in \mathbb{R}.$$

Thus, the following substitutions can be used, see [4], [34]:

$$\begin{aligned} \text{natural frequency } \omega &:= |\mu_{re}| \\ \text{decay rate } \delta &:= |\mu_{im}| \end{aligned}$$

The second differential equation is:

$$\begin{aligned} -k^4\, \frac{X''''(x)}{X(x)} + \frac{c_f}{\rho\, A} &= -\mu^2 \\ X''''(x) - \frac{\mu^2 - \frac{c_f}{\rho\, A}}{k^4} X(x) &= 0 \\ X''''(x) - \lambda^4\, X(x) &= 0, \qquad \lambda^4 := \frac{\mu^2 - \frac{c_f}{\rho\, A}}{k^4}, \end{aligned}$$

with the solution:

$$X(x) = C_3\,\cos(\lambda x) + C_4\,\sin(\lambda x) + C_5\,\cosh(\lambda x) + C_6\,\sinh(\lambda x), \quad C_3, C_4, C_5, C_6 \in \mathbb{C}.$$

Rewriting $\lambda = \lambda_{re} + i\lambda_{im}$ leads to the following (for the calculation of the root see [23]):

$$\begin{aligned}
\mu &= \sqrt{\lambda^4\,k^4 + \frac{c_f}{\rho\,A}} \\
&= \sqrt{\underbrace{k^4 \cdot (\lambda_{re}^4 + \lambda_{im}^4 - 6\lambda_{re}^2\lambda_{im}^2) + \frac{c_f}{\rho\,A}}_{=:a} + i\,\underbrace{(4\lambda_{re}^3\lambda_{im} - 4\lambda_{re}\lambda_{im}^3)}_{=:b}} \\
&= \underbrace{\sqrt{\frac{\sqrt{a^2+b^2}+a}{2}}}_{=:\mu_{re}} + i\,\underbrace{\operatorname{sign}(b)\sqrt{\frac{\sqrt{a^2+b^2}-a}{2}}}_{=:\mu_{im}}
\end{aligned}$$

therefore, the natural frequency and the decay rate is:

$$\text{natural frequency } \omega := |\mu_{re}| = \left|\sqrt{\frac{\sqrt{a^2+b^2}+a}{2}}\right| \tag{4}$$

$$\text{decay rate } \delta := |\mu_{im}| = \left|\operatorname{sign}(b)\sqrt{\frac{\sqrt{a^2+b^2}-a}{2}}\right|. \tag{5}$$

Remark 5.1. *In this chapter, a conservative system is assumed, so the energy cannot increase or decrease. Therefore, δ musst be zero and from* (5) *follows that λ must be purely real or imaginary. Both $\lambda = \lambda_{re}$ or $\lambda = i\lambda_{im}$ lead to:*

$$T(t) = C_1\,\cos(|\mu_{re}|\,t) + C_2\,\sin(|\mu_{re}|\,t).$$

Furthermore, it can be concluded:

$$\mu = \mu_{re} = \omega,$$

and for $\lambda = \lambda_{re}$

$$\omega = \sqrt{\lambda_{re}^4\,\frac{E\,I_z}{\rho\,A} + \frac{c_f}{\rho\,A}},$$

and for $\lambda = i\,\lambda_{im}$

$$\omega = \sqrt{\lambda_{im}^4\,\frac{E\,I_z}{\rho\,A} + \frac{c_f}{\rho\,A}}.$$

So $|\lambda_{re}| = |\lambda_{im}| := \lambda$ and this leads to:

$$\omega = \sqrt{\lambda^4\,\frac{E\,I_z}{\rho\,A} + \frac{c_f}{\rho\,A}}.$$

$\diamond$

All models in this section consist of four sections and, therefore, require four functions of displacement $v_i(x,t)$, $i \in 1, ..., 4$, $t \in \mathbb{R}_{>0}$:

$$\begin{aligned}
v_i(x,t) &= T_i(t) \cdot X_i(x) \\
&= \Big(C_{1i}\,\cos(\omega_i t) + C_{2i}\,\sin(\omega_i t)\Big) \cdot \Big(C_{3i}\,\cos(\lambda_i x) + C_{4i}\,\sin(\lambda_i x) \\
&\qquad + C_{5i}\,\cosh(\lambda_i x) + C_{6i}\,\sinh(\lambda_i x)\Big), \qquad i = 1, ..., 4.
\end{aligned}$$

Therefore, a relationship between ω_1, ω_2, ω_3 and ω_4 is needed. At the contact point a we have $v_i(a,t) = v_{i+1}(a,t), \forall t$, i fixed, therefore, it follows, see [34]:

$$\begin{aligned} T_i(t)X_i(a) &= T_{i+1}(t)X_{i+1}(a) \\ T_i(t) &= T_i(t)\beta \\ C_{1,i}\,\cos(\omega_i t) + C_{2,i}\,\sin(\omega_i t) &= \beta\, C_{1,i+1}\,\cos(\omega_{i+1} t) + \beta\, C_{2,i+1}\,\sin(\omega_{i+1} t). \end{aligned}$$

To accomplish this, the following must hold:

$$C_{1,i} = \beta\, C_{1,i+1} \tag{6}$$

$$C_{2,i} = \beta\, C_{2,i+1} \tag{7}$$

$$\omega_{i+1} = \omega_i + \frac{2j\pi}{t}, j \in \mathbb{Z}. \tag{8}$$

Furthermore, at the contact point we have $\dot{v}_i(a,t) = \dot{v}_{i+1}(a,t), \forall t$, and thus it follows:

$$\begin{aligned} \dot{T}_i(t) &= \dot{T}_{i+1}(t)\beta \\ -C_{1,i}\,\omega_i\,\sin(\omega_i t) + C_{2,i}\,\omega_i\,\cos(\omega_i t) &= -\beta\, C_{1,i+1}\,\omega_{i+1}\,\sin(\omega_{i+1} t) + \beta\, C_{2,i+1}\,\omega_{i+1}\,\cos(\omega_{i+1} t). \end{aligned} \tag{9}$$

If the conditions of (6)-(8) substituted in (9), this results in:

$$\begin{aligned} -\,C_{1,i}\,\omega_i\,\sin(\omega_i t) + C_{2,i}\,\omega_i\,\cos(\omega_i t) = \\ -\,C_{1,i}\left(\omega_i + \frac{2j\pi}{t}\right)\sin\Big(\left(\omega_i + \frac{2j\pi}{t}\right)t\Big) + C_{2,i}\left(\omega_i + \frac{2j\pi}{t}\right)\cos\Big(\left(\omega_i + \frac{2j\pi}{t}\right)t\Big). \end{aligned}$$

Therefrom, it follows by the comparing of the coefficients that $j = 0$ and hence $\omega_i = \omega_{i+1} := \omega$, see [34]. So, for all models we have:

$$\omega_1 = \omega_2 = \omega_3 = \omega_4 := \omega, \tag{10}$$

and the following relationship between the eigenvalues is derived:

$$\begin{aligned} \omega_1^2 &= \omega_2^2 \\ \lambda_1^4\, k^4 + \frac{c_f}{\rho\, A} &= \lambda_2^4\, k^4 \\ \lambda_2 &= \sqrt[4]{\lambda_1^4 + \frac{c_f}{E\, I_z}} \end{aligned} \tag{11}$$

$$\begin{aligned} \omega_1^2 &= \omega_3^2 \\ \lambda_3 &= \sqrt[4]{\lambda_1^4 + \frac{c_f}{E\, I_z}} \end{aligned} \tag{12}$$

$$\begin{aligned} \omega_1^2 &= \omega_4^2 \\ \lambda_4 &= \sqrt[4]{\lambda_1^4 + \frac{c_f}{E\, I_z}}, \end{aligned} \tag{13}$$

with

$$k_1^4 = k_2^4 = k_3^4 = k_4^4 := k^4. \tag{14}$$

Therefore, it follows for the four functions of displacement $v_i(x,t)$, $i \in 1, ..., 4$, $t \in \mathbb{R}_{>0}$:

$$\begin{aligned} v_1\,(x,t) = &\Big(C_{11}\,\cos\,(\omega t) + C_{21}\,\sin\,(\omega t)\Big) \cdot \Big(C_{31}\,\cos\,(\lambda x) + C_{41}\,\sin\,(\lambda x) \\ &+ C_{51}\,\cosh\,(\lambda x) + C_{61}\,\sinh\,(\lambda x)\Big),\ x \in (0, l_1) \end{aligned}$$

$$
\begin{aligned}
v_2(x,t) =& \Big(C_{12}\cos(\omega t) + C_{22}\sin(\omega t)\Big)\cdot\left(C_{32}\cos\left(\sqrt[4]{\lambda^4+\frac{c_f}{E\,I_z}}\,x\right) + C_{42}\sin\left(\sqrt[4]{\lambda^4+\frac{c_f}{E\,I_z}}\,x\right)\right.\\
&\left. + C_{52}\cosh\left(\sqrt[4]{\lambda^4+\frac{c_f}{E\,I_z}}\,x\right) + C_{62}\sinh\left(\sqrt[4]{\lambda^4+\frac{c_f}{E\,I_z}}\,x\right)\right),\ x\in(l_1,l_2)\\
v_3(x,t) =& \Big(C_{13}\cos(\omega t) + C_{23}\sin(\omega t)\Big)\cdot\left(C_{33}\cos\left(\sqrt[4]{\lambda^4+\frac{c_f}{E\,I_z}}\,x\right) + C_{43}\sin\left(\sqrt[4]{\lambda^4+\frac{c_f}{E\,I_z}}\,x\right)\right.\\
&\left. + C_{53}\cosh\left(\sqrt[4]{\lambda^4+\frac{c_f}{E\,I_z}}\,x\right) + C_{63}\sinh\left(\sqrt[4]{\lambda^4+\frac{c_f}{E\,I_z}}\,x\right)\right),\ x\in(l_2,a)\\
v_4(x,t) =& \Big(C_{14}\cos(\omega t) + C_{24}\sin(\omega t)\Big)\cdot\left(C_{34}\cos\left(\sqrt[4]{\lambda^4+\frac{c_f}{E\,I_z}}\,x\right) + C_{44}\sin\left(\sqrt[4]{\lambda^4+\frac{c_f}{E\,I_z}}\,x\right)\right.\\
&\left. + C_{54}\cosh\left(\sqrt[4]{\lambda^4+\frac{c_f}{E\,I_z}}\,x\right) + C_{64}\sinh\left(\sqrt[4]{\lambda^4+\frac{c_f}{E\,I_z}}\,x\right)\right),\ x\in(a,l).
\end{aligned}
$$

Remark 5.2. *For the models in this section, the boundary conditions (BCs) and transition conditions (TCs) are established. With Maple (Maplesoft, 2013, Version 17) a linear system in $(C_{31},...,C_{61},...,C_{34},...,C_{64})$ is derived, and with Matlab (MathWorks, 2014, Version R2014a) the solutions λ are computed, which represent the eigenvalues of the boundary-value problem (BVP). Here, only the results are shown.* ◇

Remark 5.3. *Because only the first two boundary conditions are changing, only these two new conditions of each model (Model B and C) are presented. The influence of the spring foundation is not shown, because a change of the spring rate generates only a planar shift of the χ_1-χ_2-curve ($\chi := \lambda\, l$).* ◇

5.1. Investigation of Model A

In Model A the vibrissa is held in a clamping, see Fig. 8. The discrete spring and the elastic foundation represent the skin and the FSC, respectively.

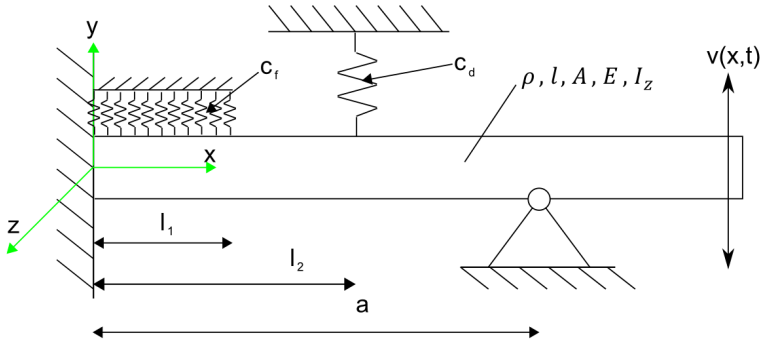

Figure 8. Model A.

For this model the following BCs and TCs, $\forall t$, are formulated:

- $v_1(0,t) = 0,\ v_1'(0,t) = 0$
- $v_1(l_1,t) = v_2(l_1,t),\ v_1'(l_1,t) = v_2'(l_1,t),\ v_1''(l_1,t) = v_2''(l_1,t),\ v_1'''(l_1,t) = v_2'''(l_1,t)$
- $v_2(l_2,t) = v_3(l_2,t),\ v_2'(l_2,t) = v_3'(l_2,t),\ v_2''(l_2,t) = v_3''(l_2,t),\ v_2'''(l_2,t) = v_3'''(l_2,t) + \frac{c_d}{E\,I_z}\,v_2(l_2,t)$
- $v_3(a,t) = v_4(a,t),\ v_3'(a,t) = v_4'(a,t),\ v_3(a,t) = 0,\ v_3''(a,t) = v_4''(a,t)$
- $v_4''(l,t) = 0,\ v_4'''(l,t) = 0$

Remark 5.4. *For the calculations, the following dimensionless ratios were introduced:*

$$
\tilde{c}_f := \frac{c_f}{\frac{E I_z}{l^4}}, \qquad \tilde{c}_d := \frac{c_d}{\frac{E I_z}{l^3}}, \qquad \tilde{a} := \frac{a}{l},
$$

and the dimensionless eigenvalue $\chi := \lambda\, l$. ◇

In Figure 9 (left), it can be seen that the contact point cannot be unambiguous determined solely by the first eigenvalue, because for a certain eigenvalue there exist two $\tilde{a}$-values. So, in a next step, it was checked, if it is possible to determine the contact point with the first two eigenvalues. Therefore, for each $\tilde{a}$-value the first and second eigenvalue are plotted in one graph. Figure 9 (right) shows, that there is no intersection of the χ_1-χ_2-curve. So it is possible to determine the contact point with the first two eigenvalues. It also can been seen, that the χ_1-χ_2-curve can be expanded with variation of the discrete spring rate.
In the next step, an algorithm is developed, which can identify the contact point with the first and second eigenvalue.

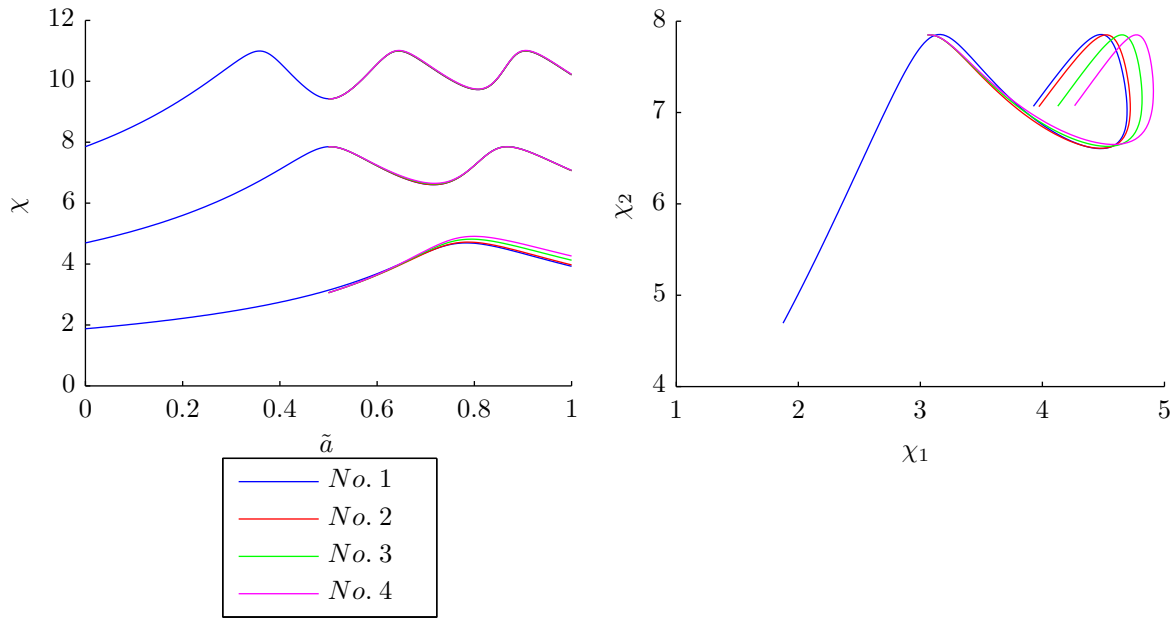

Figure 9. The first three eigenvalues for different $\tilde{c}_d$ vs. $\tilde{a}$ (left); χ_1-χ_2-curve for different $\tilde{c}_d$ (right): No. 1 $\tilde{c}_f = 0$, $\tilde{c}_d = 0$; No. 2 $\tilde{c}_f = 10$, $\tilde{c}_d = 10$; No. 3 $\tilde{c}_f = 10$, $\tilde{c}_d = 30$; No. 4 $\tilde{c}_f = 10$, $\tilde{c}_d = 50$.

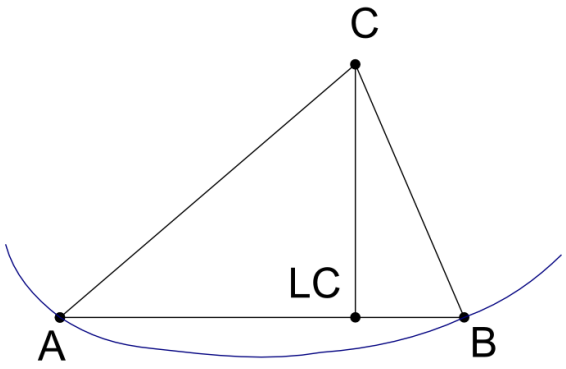

Figure 10. Geometric sketch for Algorithm 1.

Algorithm 1:
Before the algorithm can be used, a file with the values of $\tilde{a}$, χ_1 and χ_2 must be created.

1. Read values of $\tilde{a}$, χ_1 and χ_2 from the file
2. Compute for all $\tilde{a}$ from 0.5 to 1 the distance from the measured point C (χ_{1mess},χ_{2mess}) of eigenvalues (later in experiments) according to the formula:
$$d(\tilde{a}) = \sqrt{(\chi_{1mess} - \chi_1(\tilde{a}))^2 + (\chi_{2mess} - \chi_2(\tilde{a}))^2}$$

3. Determine the point B (χ_1,χ_2) with the shortest distance from C

4. Determine the point A (χ_1,χ_2) with the second shortest distance from C

5. Determine the distance $\tilde{a}(LC)$ of footpoint LC from A, see Fig. 10

6. Return the value of $\tilde{a} = \tilde{a}(A) + \tilde{a}(LC)$ ◇

Remark 5.5. *For the calculation, the values of the technical set, Table 1, is used and* $\tilde{c}_1 = 10$, $\tilde{c}_2 = 10$. ◇

To test the algorithm, it is assumed that the following eigenvalues have been measured for a chosen (and to be identified) $\tilde{a} = 0.6525$, and the step size between the calculated values for the file is $stepsize = 0.005$:

- $\chi_1 = 4.009821190665984$
- $\chi_2 = 6.836620874358188$

Table 2. Results of the Algorithm 1 - Model A.

	$\tilde{a}$	χ_1	χ_2
Algorithm 1	0.652509605326106	4.009892954566971	6.836561689590511
Difference	0.000009605326106	0.000071763900990	-0.000059184767671

Table 2 shows, that algorithm provides pretty good results for the distance detection.

5.2. Investigation of Model B

This model, see Fig. 11, differs from Model A by the support at the base. Instead of a clamping the left side is held in a bearing.

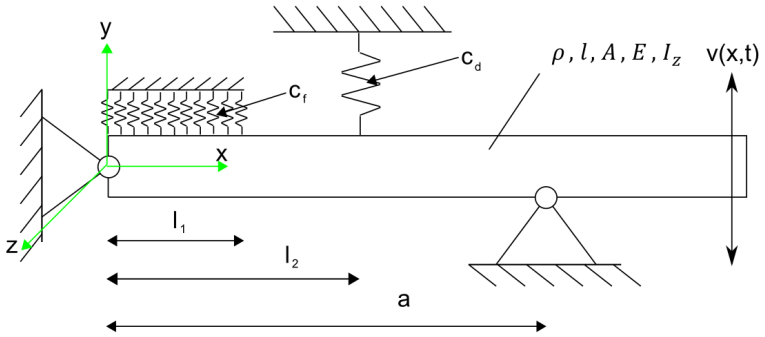

Figure 11. Model B.

The arising BCs of the new support are, $\forall t$:

- $v_1(0,t) = 0$ and $v_1''(0,t) = 0$.

Figure 12 (left) shows, that, as in Model A, an unambiguous determination of the contact point with the first eigenvalue is not possible. But, Figure 12 (right), there is an intersection of the χ_1-χ_2-curve, so also with the first and second eigenvalue an unambiguous determination of the contact point is not possible, in contrast to Model A. If the spring rate is increased the curve expands and so the intersection point vanishes. Thus, Algorithm 1 cannot be used anymore in general. Only if the spring rate is high enough (and this is not given a-priori), Algorithm 1 can unambiguous determine the contact point and thus another algorithm has to be developed, which can identify the contact point with the first, second and third eigenvalue.

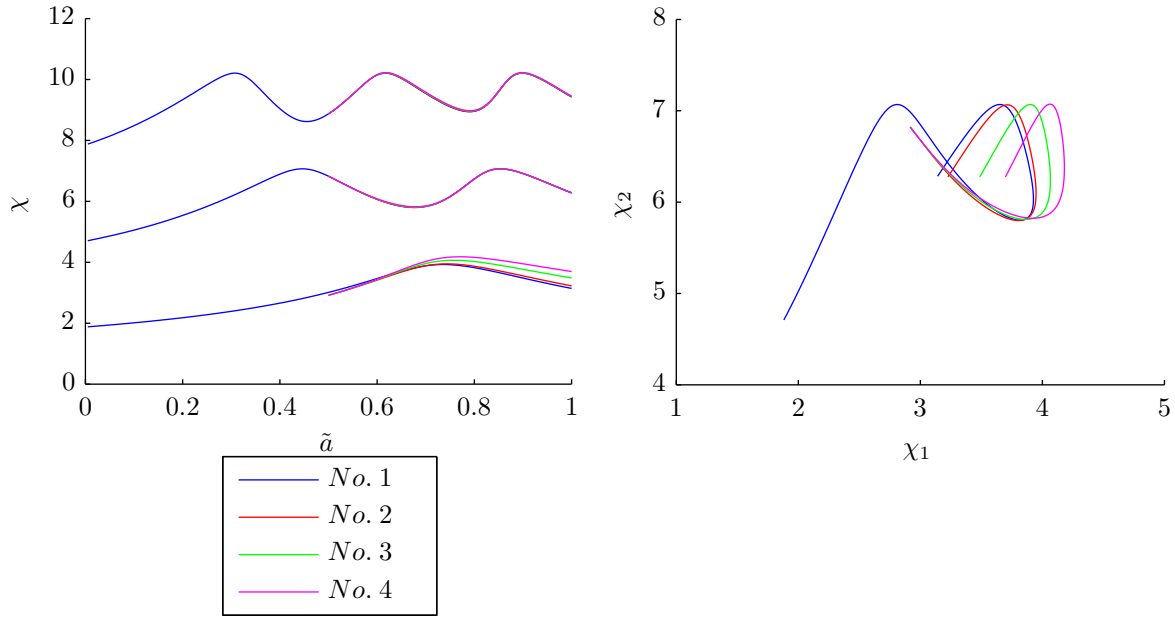

Figure 12. The first three eigenvalues for different $\tilde{c}_d$ vs. $\tilde{a}$ (left); χ_1-χ_2-curve for different $\tilde{c}_d$ (right): No. 1 $\tilde{c}_f = 0$, $\tilde{c}_d = 0$; No. 2 $\tilde{c}_f = 10$, $\tilde{c}_d = 10$; No. 3 $\tilde{c}_f = 10$, $\tilde{c}_d = 30$; No. 4 $\tilde{c}_f = 10$, $\tilde{c}_d = 50$.

Remark 5.6. *In Matlab (MathWorks, 2014, Version R2014a) the χ_1-χ_2-χ_3-curve is plotted. There was no intersection point and so an unambiguous determination of the contact point with the first three eigenvalues is possible.* ◇

Algorithm 2:
Before the algorithm can be used, a file with the values of $\tilde{a}$, χ_1, χ_2 and χ_3 must be created.

1. Read values of $\tilde{a}$, χ_1, χ_2 and χ_3 from the file
2. Compute for all $\tilde{a}$ from 0.5 to 1 the distance from the measured point C (χ_{1mess},χ_{2mess},χ_{3mess}) of eigenvalues (later in experiments) according to the formula:
$$d(\tilde{a}) = \sqrt{(\chi_{1mess} - \chi_1(\tilde{a}))^2 + (\chi_{2mess} - \chi_2(\tilde{a}))^2 + (\chi_{3mess} - \chi_3(\tilde{a}))^2}$$
3. Determine the point B (χ_1,χ_2,χ_3) with the shortest distance from C
4. Determine the point A (χ_1,χ_2,χ_3) with the second shortest distance from C
5. Determine the distance $\tilde{a}(LC)$ of footpoint LC from A
6. Return the value of $\tilde{a} = \tilde{a}(A) + \tilde{a}(LC)$ ◇

Remark 5.7. *For the calculation the values of the technical set, Table 1, is used and $\tilde{c}_1 = 10$, $\tilde{c}_2 = 30$.* ◇

To test these two algorithms, it is assumed that the following eigenvalues have been measured for a given (and to identified) $\tilde{a} = 0.6525$ and the step size of calculated values for the file is $stepsize = 0.005$:

- $\chi_1 = 3.731967524287328$
- $\chi_2 = 5.844390565285849$
- $\chi_3 = 10.033242682221617$

Table 3. Results of the Algorithm 2 - Model B.

	$\tilde{a}$	χ_1	χ_2	χ_3
Algorithm 2	0.652484098410265	3.731877648391381	5.844431508913212	10.033242682221617
Difference:	-0.000016254322481	-0.000089875895940	0.000040943627370	0.000142676864199

Table 4. Results of the Algorithm 1 - Model B.

	$\tilde{a}$	χ_1	χ_2
Algorithm 1	0.652526752659562	3.732115438706637	5.844323226138748
Difference:	0.00002675265956	0.00014791441931	-0.00006733914710

If Table 3 is compared with Table 4, it is apparent that Algorithm 2 works better for this model than Algorithm 1. But, this difference is small and both lead to the requested value if the results are rounded to four digits.

5.3. Investigation of Model C

This model, see Fig. 13, differs from Model A and B by the support at the base. Instead of a clamping or a bearing the left side is free.

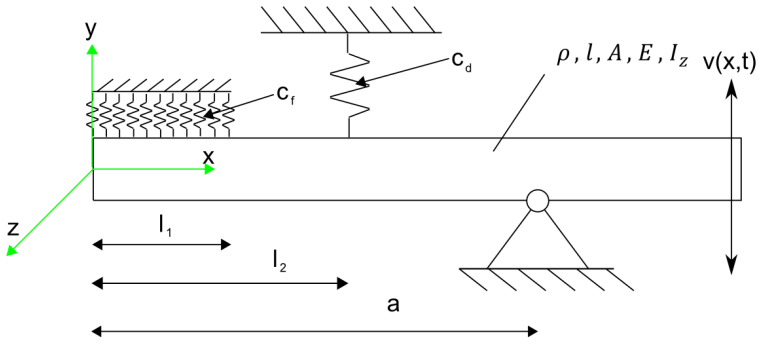

Figure 13. Model C.

The arising BCs are, $\forall t$:

- $v_1''(0,t) = 0$ and $v_1'''(0,t) = 0$.

Figure 14 shows, that, as in Model B, an unambiguous determination of the contact point with the first eigenvalue and with the first an second eigenvalue is not possible. As in Model B, if the spring rate is increased the curve expands and so the intersection point of the χ_1-χ_2-χ_3-curve vanishes. Only if the spring rate is high enough, Algorithm 1 can unambiguous determine the contact point and so in general Algorithm 2 has to be used.

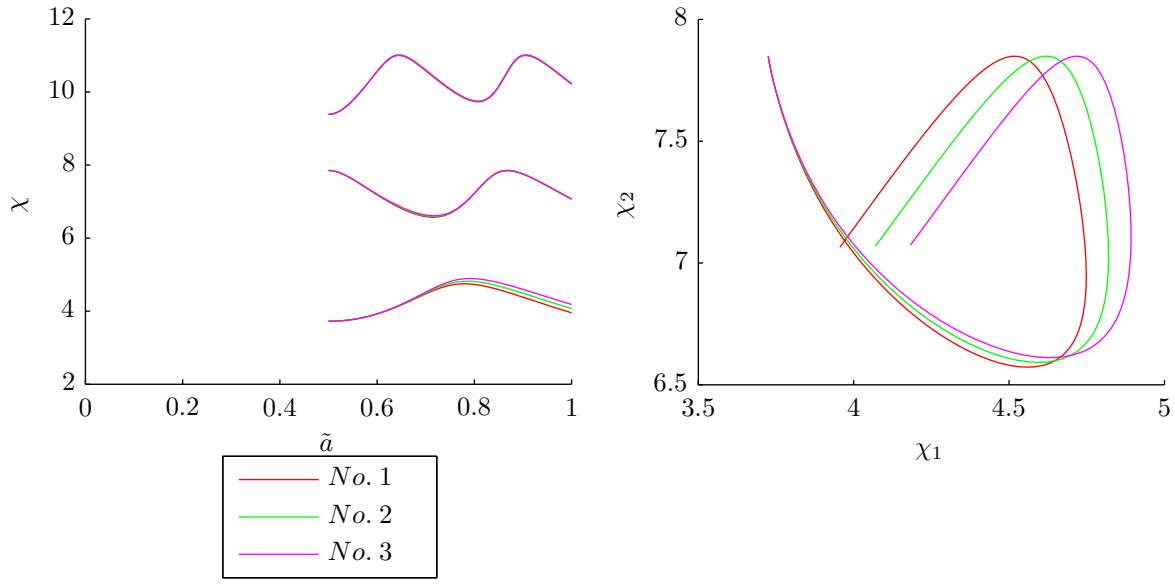

Figure 14. The first three eigenvalues for different $\tilde{c}_d$ vs. $\tilde{a}$ (left); χ_1-χ_2-curve for different $\tilde{c}_d$ (right): No. 1 $\tilde{c}_f = 10$, $\tilde{c}_d = 10$; No. 2 $\tilde{c}_f = 10$, $\tilde{c}_d = 30$; No. 3 $\tilde{c}_f = 10$, $\tilde{c}_d = 50$.

Remark 5.8. *For the calculation the values of the technical set, Table 1, is used and* $\tilde{c}_1 = 10$, $\tilde{c}_2 = 30$. $\diamond$

To test both algorithms, it is assumed that the following eigenvalues have been measured for a given (but to be identified) $\tilde{a} = 0.6525$ (the step size of the calculated values for the file is $stepsize = 0.005$):

- $\chi_1 = 4.194420266332767$
- $\chi_2 = 6.811788900720613$
- $\chi_3 = 10.991851216321621$

Table 5. Results of the Algorithm 2 - Model C.

	$\tilde{a}$	χ_1	χ_2	χ_3
Algorithm 2	0.652457474802077	4.194165392853138	6.812044228850565	10.991996397898973
Difference:	-0.000042525197923	-0.000254873479630	0.000255328129950	0.000145181577301

Table 6. Results of the Algorithm 1 - Model C.

	$\tilde{a}$	χ_1	χ_2
Algorithm 1	0.652508007451328	4.194468264239080	6.811740834385314
Difference:	0.00000800745133	0.00004799790632	-0.00004806633530

If Table 5 is compared with Table 6, it is shown that Algorithm 1 works better for this model than Algorithm 2 (but the intersection cannot be excluded a-priori). But, both lead to the requested value if the results are rounded to four digits.

6. SUMMARY AND FUTURE PROSPECTS

The scope of the present paper was to contribute to the mechanical modeling of technical vibrissa as tactile sensors for the distance detection. Here, the focus is not on using the mechanical model to explain the characteristics and functions of the biological system of the vibrissae, but on the investigation of the relationship and properties of the technical system.
As a first step, the modeling of the vibrissa was considered. It was shown, which parts of the vibrissa can be modeled by means of mechanical components. Subsequently, three models were built and for the technical vibrissa a set of parameters was presented.
In a next step, three conservative models have been analyzed. For all models, a distance detection with only the first eigenvalue was not possible. But, for Model A is an unambiguous distance detection with the first two eigenvalues possible and with the discrete spring the χ_1-χ_2-curve could be expand and so the accuracy can be increased. So, a first algorithm was developed, which can determine the distance with a file of the first two eigenvalues. But, for Model B and C, this algorithm cannot be used in general, because an unambiguous distance detection with the first two eigenvalues is not possible for all parameters of the system. It was shown, that with the discrete spring the χ_1-χ_2-curve could be expand, so that the intersection points vanishes. But, one goal was to develop an algorithm that can be used for all models independent on the parameters of the system. It was found, that for all models an unambiguous distance detection with the first three eigenvalues is possible. So, a second algorithm was developed, which can determine the distance with a file of the first three eigenvalues. The first algorithm was tested for Model A, B and C, and the second one for Model B and C. It was found that both algorithms provide good results.
Future steps should be directed to:

- investigation of Model A, B and C with various cross sections,
- investigation of Model A, B and C with a discrete damper,
- investigation of Model A, B and C with a damper foundation.

But, also some of the conditions and assumptions of Chapter 5 could be dropped. The vibrissa has a pre-curvature, so investigation on beams with a pre-curvature should be done, or E, ρ, A and I_z are no longer constant over the length of the beam.

7. REFERENCES

[1] Ahl, A. S. (1986): The role of vibrissae in behavior: a status review; in: *Veterinary research communications* **10**(4), pp. 245-268.

[2] Behn, C. (2013a): Modeling the Behavior of Hair Follicle Receptors as Technical Sensors using Adaptive Control; in: *Proceedings of 10th International Conference on Informatics in Control, Automation and Robotics* (ICINCO 2013), Reykjavík (Iceland), pp. 336-345, SciTePress, DOI:10.5220/0004488003360345.

[3] Behn, C., T.A. Schmitz, H. Witte, and K. Zimmermann (2013b): Animal Vibrissae: Modeling and Adaptive Control of bio-inspired Sensors; in: *Proceedings of 12th International Work-Conference on Artificial Neural Networks* (IWANN 2013), Editors: I. Rojas, G. Joya, and J. Cabestany, Part II, Lecture Notes in Computer Science (LNCS) 7903 (Advances in Computational Intelligence), Springer, Berlin, pp. 159-170.

[4] Behn, C. (2013c): Mathematical modeling and control of biologically inspired uncertain motion systems with adaptive features; TU Ilmenau, Faculty of Mechanical Engineering, habilitation thesis.

[5] Behn, C., C. Will, and J. Steigenberger (2014): Unlike Behavior of Natural Frequencies in Bending Beam Vibrations with Boundary Damping in Context of Bio-inspired Sensors; in: *Proceedings of the Third International Conference on Intelligent Systems and Applications* (INTELLI 2014), Sevilla (Spain), pp. 75-84, IARIA, ISBN 978-1-61208-352-0.

[6] Berg, R. W. and D. Kleinfeld (2003): Rhythmic Whisking by Rat: Retraction as Well as Protraction of the Vibrissae Is Under Active Muscular Control; in: *Journal of neurophysiology* **89**(1), pp. 104-117.

[7] Birdwell, J. A., J. H. Solomon, M. Thajchayapong, M. A. Taylor, M. Cheely, R. B. Towal, J. Conradt and M. J. Hartmann (2007): Biomechanical Models for Radial Distance Determination by the Rat Vibrissal System; in: *Journal of Neurophysiology* **98**(4), pp. 2439-2455.

[8] Carl, K. (2009): Technische Biologie des Tasthaar-Sinnessystems als Gestaltungsgrundlage für taktile stiftführende Mechanosensoren (Technical biology of the vibrissa-sensory system as a design basis for tactile pin-leading mechanosensors); TU Ilmenau, PhD thesis.

[9] Carl, K., W. Hild, J. Mämpel, C. Schilling, R. Uhlig and H. Witte (2012): Characterization of Statical Properties of Rat's Whisker System; in: *IEEE Sensors Journal* **12**(2), pp. 340-349.

[10] Dörfl, J. (1982): The musculature of the mystacial vibrissae of the white mouse; in: *Journal of anatomy* **135**, pp. 147-154.

[11] Dubbel, H. (2007): Taschenbuch für den Maschinenbau (Paperback for Mechanical Engineering), 22nd edition, Berlin, Heidelberg and New York: Springer.

[12] Fundin, B. T., J. Arvidsson and F. L. Rice (1995): Innervation of nonmystacial vibrissae in the adult rat; in: *The Journal of Comparative Neurology* **357**(4), pp. 501-512.

[13] Gasch, R., K. Knothe and R. Liebich (2012): Strukturdynamik: Diskrete Systeme und Kontinua (Structural Dynamics: discrete systems and continua), 2nd edition, Berlin and Heidelberg: Springer.

[14] Gopal, V. and M. J. Hartmann (2007): Using hardware models to quantify sensory data acquisition across the rat vibrissal array; in: *Bioinspiration & Biomimetics* **2**(4), pp. 135-145.

[15] Gross, D., W. Hauger, J. Schröder and W. A. Wall (2014): Technische Mechanik 2: Elastostatik (Technical Mechanics 2: Elastostatics), 12th edition, Berlin and Heidelberg: Springer.

[16] Halata, Z. (1993): Sensory innervation of the hairy skin (light- and electronmicroscopic study); in: *The Journal of investigative dermatology* **101**, pp. 75-81.

[17] Hartmann, M. J., N. J. Johnson, R. B. Towal and C. Assad (2003): Mechanical characteristics of rat vibrissae: resonant frequencies and damping in isolated whiskers and in the awake behaving animal; in: *The Journal of neuroscience* **23**(16), pp. 6510-6519.

[18] Holzmann, G. (2011): Technische Mechanik: Festigkeitslehre (Technical Mechanics: Elasticity), 10th edition, Wiesbaden: Teubner.

[19] Kim, D. and R. Möller (2004): A biomimetic whisker for texture discrimination and distance estimation; in: *From Animals to Animats* **8**, pp. 140-149.

[20] Krehbiehl, M. (2010): Anatomie der rostralen und caudalen Tasthaare beim Sambischen Riesengraumull (Fukomys mechowii) : Sinushaare oder Leithaare? (Anatomy of the rostral and caudal vibrissae in the zambian mechow's mole rat (Fukomys mechowii): sinus hairs or guard hairs?); Tierärztliche Hochschschule Hannover, PhD thesis.

[21] Liebich, H.-G. (2010): Funktionelle Histologie der Haussäugetiere und Vögel (Functional histology of domestic mammals and birds), 5th Edition, Stuttgart and New York: Schattauer.

[22] Merkel, M. and A. Öchsner (2010): Eindimensionale finite Elemente: Ein Einstieg in die Methode (One-dimensional Finite Elements: An introduction to the method), Berlin and Heidelberg: Springer.

[23] Meyberg, Kurt and Peter Vachenauer (2006): Höhere Mathematik 2: Differentialgleichungen, Funktionentheorie, Fourier-Analysis, Variationsrechnung (Higher Mathematics 2: differential equations, function theory, Fourier analysis, calculus of variations), 4th Edition, Berlin: Springer.

[24] Neimark, M. A., M. L. Andermann, J. J. Hopfield and C. I. Moore (2003): Vibrissa Resonance as a Transduction Mechanism for Tactile Encoding; in: *The journal of neuroscience* **23**(16), pp. 6499-6509.

[25] N'Guyen, S., P. Pirim and J.A. Meyer (2010): Tactile texture discrimination in the robot rat psikharpax; in: *BIOSIGNALS 2010, 3rd International Conference on Bio-inspired Systems and Signal Processing*, pp. 74-81.

[26] Rao, S. (2007): Vibration of continuous systems, Hoboken and N.J.: Wiley.

[27] Salomon, F.-V., Hrsg. (2008): Anatomie für die Tiermedizin (Anatomy for veterinary medicine), 2nd Edition, Stuttgart: Enke.

[28] Schmitz, T. and C. Behn (2011a): Analytical Investigations and Adaptive Control of Vibrissae-like Sensor Models with Finite DoF; in: *Proceedings of 56th Internationales Wissenschaftliches Kolloquium*, Ilmenau (Germany).

[29] Schmitz, T. (2011b): Entwurf und Analyse von biologisch inspirierten Sensorsystemen mit erhöhtem Freiheitsgrad am Beispiel Vibrisse (Design and analysis of biologically-inspired sensor systems with a higher degree of freedom on the example of the vibrissa); TU Ilmenau, MSc. thesis.

[30] Scholz, G. R. and C. D. Rahn (2004): Profile Sensing With an Actuated Whisker; in: *IEEE Transactions on Robotics and Automation* **20**(1), pp. 124-127.

[31] Schultz, A. E., J. H. Solomon, M. A. Peshkin and M. J. Hartmann (2005): Multifunctional Whisker Arrays for Distance Detection, Terrain Mapping, and Object Feature Extraction; in: *Proceedings of the 2005 IEEE International Conference on Robotics and Automation*, pp. 2588-2593.

[32] Ueno, N., M. M. Svinin and M. Kaneko (1998): Dynamic contact sensing by flexible beam; in: *IEEE/ASME Transactions on Mechatronics* **3**(4), pp. 254-264.

[33] Voges, D., K. Carl, G. J. Klauer, R. Uhlig, C. Schilling, C. Behn and H. Witte (2012): Structural Characterization of the Whisker System of the Rat; in: *IEEE Sensors Journal* **12**(2), pp. 332-339.

[34] Will, C. (2012): Beiträge zu kontinuierlichen Schwingungssystemen: Schwingungen abgesetzter Balken mit diskreten Elementen (Contributions to continuous vibration systems: vibrations of stepped beams with discrete elements); TU Ilmenau, BSc. thesis.

[35] Wriggers, P. (2006): Technische Mechanik kompakt: Starrkörperstatik, Elastostatik, Kinetik (Technical mechanics compact: Rigid body statics, elastostatics, Kinetics), 2nd edition, Wiesbaden: Teubner.

[36] Yan, W., Q. Kan, K. Kergrene, G. Kang, X.-Q. Feng and R. Rajan (2013): A truncated conical beam model for analysis of the vibration of rat whiskers; in: *Journal of biomechanics* **46**(12), pp. 1987-1995.